Enhanced robustness properties and tracking performance of the quadrotor unmanned aerial vehicle under disturbances via the second order sliding mode control

Faik Tahirovic, Almir Salihbegovic, Emir Sokic and Nedim Osmic[1]

***Abstract*— This paper presents a full degrees-of-freedom (DOFs) robust control design for a nonlinear quadrotor unmanned aerial vehicle (UAV) operating under bounded disturbances. Second-order sliding modes controllers (SOSMCs) are designed so that the quadrotor UAV can follow a 3D trajectory in the presence of model uncertainties, underactuation, as well as external disturbances that may be matched or mismatched, and vanishing or nonvanishing. The stability analysis of the closed-loop system is presented via the Lyapunov method, showing the finite-time convergence of the system trajectories to the sliding surfaces, as well as the finite-time convergence of the quadrotor position and attitude to their reference values. The high-gain adaptation (HGA) method is adopted in the SOSMC technique, called SOSMC-HGA, to alleviate the chattering phenomenon. Simulation studies in different scenarios demonstrate that the SOSMC technique exhibits superior tracking performance and robustness properties compared to concurrent control methods for tracking reference trajectories of quadrotor UAVs. The simulation results confirm that SOSMC-HGA significantly attenuates the chattering phenomenon in control signals and system states, which is an important improvement, as it increases the safety of UAVs and reduces power consumption.**

I. Introduction

The concept of multi-rotor aerial vehicles (MAVs) was introduced into aerial robotics more than two decades ago [1], [2]. Recently, there has been significant interest in MAVs, particularly quadrotor platforms, representing unmanned aerial vehicles (UAVs) with four rotors. The dynamics of MAVs is typically nonlinear and strongly cross-coupled, making them highly vulnerable to different uncertainties and disturbances. Consequently, designing control strategies for such systems is a quite challenging task. However, MAVs offer several advantages over conventional helicopters [3]–[5], including simple construction, excellent maneuverability, high payload capacity, and low-cost maintenance [6]. Furthermore, advances in electronics, light materials, batteries, and sensors in recent decades have allowed MAVs to be equipped with a wide range of equipment without a significant impact on their payload [1].

Initial implementations of various control methods, such as the PID controller, the linear-quadratic regulator (LQR), the backstepping and the sliding mode control (SMC), for unmanned operations of micro-quadrators were first introduced in [1] and [7]. Subsequently, improvements have been made in the control design of MAVs, enabling them to perform aggressive maneuvers [8]–[10] and complex operations [11]. Due to their ability to perform vertical take-off and landing (VTOL) [12], as well as operate in indoor and outdoor environments [13], [14], MAVs are extensively used in various civil and military applications [15], including rescue operations [16], surveillance, fault detection [17], [18], inspection tasks [19], monitoring [20], mapping and localization [21], navigation in unknown environments [22], and serving as educational platforms [23], among others.

Additionally, quadrotor UAVs are characterized as underactuated systems with four controlled variables (thrust and three moments) and six actual outputs (position and orientation coordinates). These systems have fewer controlled variables than DOFs, making them suitable for applications (in aerial, underwater, or space robotics) that require weight reduction, cost efficiency, and energy conservation. However, designing control strategies for underactuated systems is challenging, as it is typically not possible to use smooth feedback to locally stabilize their states [24]. As a result, SMC methods have been implemented to robustly stabilize quadrotors affected by disturbances and uncertainties [6], [24]–[27]. Nevertheless, previous studies [6], [24], [25], [27], [28] have used simplified quadrotor models to evaluate the performance of SMCs, or even adjust initial conditions to eliminate the reaching phase and consequently avoid the chattering phenomenon [6], [24], [26], [27].

The aim of this paper is to develop a robust full DOFs (position and orientation coordinates) control technique based on the second-order sliding mode (SOSM) for tracking 3D trajectories of quadrotor UAVs affected by various disturbances. The highly nonlinear dynamics of the quadrotor is obtained using a generalized framework for MAV modeling [29], [30]. Stability analysis and control design are conducted using the Lyapunov method. Accordingly, the designed SOSMC ensures the finite-time convergence of the closed-loop system trajectories to the sliding surface. In addition to the first-order SMC (FOSMC) for tracking 3D trajectories of MAVs [31], [32], it also guarantees finite-time convergence of the quadrotor position and orientation to their desired values. Thereby, the flat mapping [30] between Cartesian coordinates (x, y) and Euler's roll and pitch angles (ϕ, θ) is incorporated into SOSMC, simplifying the closed-loop control design. This approach provides convergence not only of UAV attitude tracking errors in finite-time as in [33], [34], but also of the quadrotor position tracking errors. Moreover, the HGA algorithm is effectively included in the SOSMC scheme,

[1]All authors are with Department for Automatic Control and Electronics, Faculty of Electrical Engineering, University of Sarajevo, 71000 Sarajevo, Bosnia and Herzegovina, almir.salihbegovic@etf.unsa.ba

where the switching control gain increases during the reaching phase, that is, before the sliding surface is reached, and then the switching gain starts to decrease. Therefore, the SOSMC-HGA approach does not require the use of disturbance estimators [35] or robust internal loop compensators (RICs) [36] for chattering attenuation due to reduced switching control gain in SMs. The proposed SOSM-based control scheme will demonstrate through simulation studies an excellent ability to track the reference trajectories of the quadrotor UAV exposed to various uncertainties and disturbances. Comparison analysis with concurrent results [31], [32] will be presented in terms of the robustness and tracking performance of the control system to track the trajectory.

The structure of the paper is as follows. Section II presents the highly nonlinear mathematical model of a quadrotor UAV using a generalized framework for MAV modeling. Section III describes a detailed control design procedure based on SOSMs for robust stabilization of the quadrotor UAV. The effects of external disturbances on the quadrotor UAV are analyzed in Section IV through several simulation scenarios. The paper ends with the conclusion remarks in Section V.

II. Kinematics and Dynamics of the Quadrotor UAV

The quadrotor UAV discussed in this paper is conceptualized as a structurally rigid entity, consisting of four propellers driven by four DC motors positioned symmetrically. In addition to the symmetric arrangement of the propellers, the rotors adopt a balanced PNPN configuration (positive-negative-positive-negative) [30]. This configuration ensures that propellers 1 and 3 perform rotations in the positive direction, while propellers 2 and 4 spin in the negative direction. For visual reference, the UAV is shown in Fig. 1. The control module is strategically placed at the central hub of the quadrotor, establishing a direct connection to each propeller through uniform-length arms, denoted l. In addition to defining the physical structure of the UAV, the coordinate axes X, Y, and Z are introduced, aligning with the spatial orientation. Each rotor generates a distinct force, labeled F_i, where $i = 1, 2, 3, 4$. These forces are mathematically expressed as $F_i = b\Omega_i^2$, where b represents the constant of motor thrust (consistent across all motors) and Ω_i denotes the angular velocity of the i-th motor. The force vector that acts on the body of the quadrotor is defined as $\mathbf{F} = \mathbf{F}_G^B + \mathbf{T}(\in \mathbb{R}^3)$, where $\mathbf{F}_G^B$ is the gravitational force vector, while $\mathbf{T}$ is the thrust vector. The thrust vector $\mathbf{T}$ represents the sum of all forces consequential of the rotation of the propellers and is assumed to only have a non-zero value in the direction of the Z axis, so it can be written as $\mathbf{T} = \begin{bmatrix} 0 & 0 & T_z \end{bmatrix}^T$, where thrust T_z along the Z axis is

$$T_z = \sum_{i=1}^{4} F_i = b \sum_{i=1}^{4} \Omega_i^2. \tag{1}$$

The propellers were directed and placed so that rotation around the X axis is achieved solely by forces F_1 and F_3, while rotation around the Y axis is obtained solely by forces F_2 and F_4. The drag moment of motor i is defined as $M_i = d\Omega_i^2$ for the corresponding axis, where d is the drag constant of the rotor. The moment vector is now defined as

$$\tau = \begin{bmatrix} \tau_x \\ \tau_y \\ \tau_z \end{bmatrix} = \begin{bmatrix} bl(\Omega_1^2 - \Omega_3^2) \\ bl(\Omega_4^2 - \Omega_2^2) \\ d(\Omega_2^2 + \Omega_4^2 - \Omega_1^2 - \Omega_3^2) \end{bmatrix}. \tag{2}$$

Virtual control vector $\mathbf{u} \in \mathbb{R}^4$ can be expressed as

$$\mathbf{u} = \begin{bmatrix} T_z & \tau \end{bmatrix}^T = \begin{bmatrix} T & \tau_x & \tau_y & \tau_z \end{bmatrix}^T = \mathbf{A}\boldsymbol{\Omega}_\mathbf{s}, \tag{3}$$

where vector $\boldsymbol{\Omega}_\mathbf{s} \in \mathbb{R}^4$ of angular speed of rotors, represented by

$$\boldsymbol{\Omega}_\mathbf{s} = \begin{bmatrix} \Omega_1^2 & \Omega_2^2 & \Omega_3^2 & \Omega_4^2 \end{bmatrix}^T, \tag{4}$$

is the only controllable variable, while actuation matrix $\mathbf{A} \in \mathbb{R}^{4\times4}$ is responsible for transforming angular speed to virtual control as follows

$$\mathbf{A} = \begin{bmatrix} b & b & b & b \\ bl & 0 & -bl & 0 \\ 0 & -bl & 0 & bl \\ -d & d & -d & d \end{bmatrix}. \tag{5}$$

To provide an accurate description of the quadrotor system, it is essential to determine the relations between the local coordinate system XYZ and the global coordinate system $X_BY_BZ_B$. The local coordinate system is introduced as ENU system (Cartesian xEast, yNorth, zUp). Position vector $\mathbf{x} = \begin{bmatrix} x & y & z \end{bmatrix}^T$ is used to describe the position of the UAV, and since a rigid body has six DOFs in a 3D space, it is also necessary to use vector $\boldsymbol{\Psi} = \begin{bmatrix} \phi & \theta & \psi \end{bmatrix}^T$ of Euler's angles to describe a quadrotor's orientation. Furthermore, in order to keep the notation short s_α will represent $\sin(\alpha)$ while c_α will denote $\cos(\alpha)$ for any angle α. Now, the rotation matrix $\mathbf{R}$ which transforms from local to global coordinate system is [31] .

$$\mathbf{R}(\phi, \theta, \psi) = \begin{bmatrix} c_\theta c_\psi & s_\phi s_\theta c_\psi - c_\phi s_\psi & c_\phi s_\theta c_\psi + s_\phi s_\psi \\ c_\theta s_\psi & s_\phi s_\theta s_\psi + c_\phi c_\psi & c_\phi s_\theta s_\psi - s_\phi c_\psi \\ -s_\theta & s_\phi c_\theta & c_\phi s_\theta \end{bmatrix}. \tag{6}$$

This matrix now defines the relationship between the velocity vector in the global coordinate system $\dot{\mathbf{x}} = \begin{bmatrix} \dot{x} & \dot{y} & \dot{z} \end{bmatrix}^T$ and linear velocity vector in the local coordinate system $\mathbf{v} = \begin{bmatrix} u & v & w \end{bmatrix}^T$ as $\dot{\mathbf{x}} = \mathbf{R}(\phi, \theta, \psi)\mathbf{v}$. Moreover, angular velocity vector in the local frame $\mathbf{P} = \begin{bmatrix} P & Q & R \end{bmatrix}^T$ is connected with rotational velocity vector $\dot{\boldsymbol{\Psi}} = \begin{bmatrix} \dot{\phi} & \dot{\theta} & \dot{\psi} \end{bmatrix}^T$ as

$$\dot{\boldsymbol{\Psi}} = \mathbf{R}_A^{-1}(\phi, \theta, \psi)\mathbf{P}, \tag{7}$$

where inverse of the angular rotation matrix can be derived as [31]

$$\mathbf{R}_A^{-1}(\phi, \theta, \psi) = \begin{bmatrix} 1 & s_\phi t_\theta & s_\phi t_\theta \\ 0 & c_\phi & -s_\phi \\ 0 & \frac{s_\phi}{c_\theta} & \frac{c_\phi}{c_\theta} \end{bmatrix}. \tag{8}$$

Applying D'Alembert's principle yields the following

$$\mathbf{S}m\mathbf{v} + m\dot{\mathbf{v}} - \mathbf{T} - \mathbf{F}_G^B = 0. \tag{9}$$

Solving (9) with respect to $\dot{\mathbf{v}}$ follows

$$\dot{\mathbf{v}} = -\mathbf{S}\mathbf{v} + \frac{\mathbf{T}}{m} + \frac{\mathbf{F}_G^B}{m}, \tag{10}$$

where m represents a total mass of the quadrotor and $\mathbf{S} \in \mathbb{R}^{3\times3}$ is a skew-symmetric matrix consisting of angular velocities [30]

$$\mathbf{S} = \begin{bmatrix} 0 & -R & Q \\ R & 0 & -P \\ -Q & P & 0 \end{bmatrix}. \tag{11}$$

The gravitational force vector $\mathbf{F}_G^B \in \mathbb{R}^3$ can be expressed in the global coordinate system as .

$$\mathbf{F}_G^B = \begin{bmatrix} 0 & -R & Q \\ R & 0 & -P \\ -Q & P & 0 \end{bmatrix} \cdot \begin{bmatrix} 0 \\ 0 \\ mg \end{bmatrix} = mg \begin{bmatrix} s_\theta \\ -s_\phi c_\theta \\ -c_\phi c_\theta \end{bmatrix}, \tag{12}$$

where g denotes the acceleration of gravity. By defining the matrix of the inertia tensor as $\mathbf{J} = \text{diag}(I_{xx}, I_{yy}, I_{zz})$, where the moments of inertia I_{xx}, I_{yy}, I_{zz} around each axis are obtained using the Huygens-Steiner theorem [30], the dynamics of angular motion can be described as

$$\dot{\mathbf{P}} = \mathbf{J}^{-1}(\tau - \mathbf{S}\mathbf{J}\mathbf{P}). \tag{13}$$

Now, the full state-space model of the quadrotor UAV is described using (10) and (13) as follows .

$$\dot{x} = c_\theta c_\psi u + \left(s_\phi s_\theta c_\psi - c_\phi s_\psi\right) v + \left(c_\phi s_\theta c_\psi + s_\phi s_\psi\right) w \tag{14}$$
$$\dot{y} = c_\theta s_\psi u + \left(s_\phi s_\theta s_\psi + c_\phi c_\psi\right) v + \left(c_\phi s_\theta s_\psi - s_\phi c_\psi\right) w \tag{15}$$
$$\dot{z} = -s_\theta u + s_\phi c_\theta v + c_\phi c_\theta w \tag{16}$$
$$\dot{u} = Rv - Qw + gs_\theta \tag{17}$$
$$\dot{v} = Pw - Ru - gs_\phi c_\theta \tag{18}$$
$$\dot{w} = Qu - Pv - gc_\phi c_\theta + \frac{T}{m} \tag{19}$$
$$\dot{P} = \frac{I_{yy} - I_{zz}}{I_{xx}} QR + \frac{\tau_x}{I_{xx}} - \frac{I_{zzm}}{I_{xx}} QW_G \tag{20}$$
$$\dot{Q} = \frac{I_{zz} - I_{xx}}{I_{xx}} PR + \frac{\tau_y}{I_{yy}} - \frac{I_{zzm}}{I_{yy}} PW_G \tag{21}$$
$$\dot{R} = \frac{I_{xx} - I_{yy}}{I_{zz}} PQ + \frac{\tau_z}{I_{zz}} \tag{22}$$
$$\dot{\phi} = P + Qs_\phi t_\theta + Rc_\phi t_\theta \tag{23}$$
$$\dot{\theta} = Qc_\phi - Rs_\phi \tag{24}$$
$$\dot{\psi} = Q\frac{s_\phi}{c_\theta} + R\frac{c_\phi}{c_\theta} \tag{25}$$

More details regarding the kinematics and dynamics of quadrotors, based on the generalized framework for modeling of MAVs, can be accessed in our previous work [29]–[32], [37].

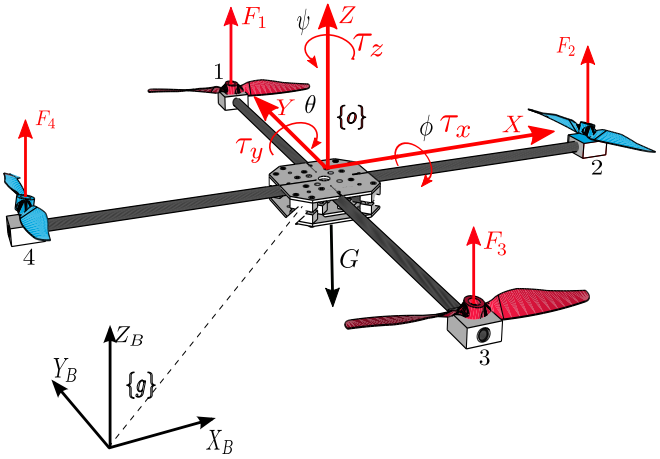

Fig. 1: Forces and moments acting on the quadrotor UAV

III. Design of the SOSMC for Trajectory Tracking of a Quadrotor UAV

This section presents the control design strategy based on the second order SMs for a robust stabilization of the quadrotor UAV operating under various bounded disturbances. Controllers are designed so that the quadrotor UAV is able to follow a 3D trajectory in the presence of modeling and parametric uncertainties, as well as bounded external disturbances, that may be matched or mismatched, as well as vanishing or nonvanishing.

A. SOSM based altitude control of the quadrotor UAV

Consider the altitude tracking error e_z as

$$e_z = z - z_{ref}, \tag{26}$$

and the altitude sliding variable σ_z as

$$\sigma_z = \dot{e}_z + c_z |e_z|^{\frac{1}{2}} \text{sgn}(e_z), \tag{27}$$

where z_{ref} represents the altitude reference and c_z is a positive constant. The altitude sliding manifold

$$\sigma_z = \dot{e}_z + c_z |e_z|^{\frac{1}{2}} \text{sgn}(e_z) = 0 \tag{28}$$

ensures the nonlinear and continuous altitude phase trajectory in the phase plane, despite the presence of the switching function $\text{sgn}(\sigma_z)$. A candidate Lyapunov function is chosen as

$$V_z = \frac{\sigma_z^2}{2}, \tag{29}$$

representing a positive definite and continuously differentiable function. The first derivative of (29) is negative definite if the following condition of finite-time convergence [32]

$$\dot{\sigma}_z + \beta_z \text{sgn}(\sigma_z) = 0 \tag{30}$$

holds, where β_z is a positive constant. Indeed, using (30) and calculating the derivative of (29) along the system trajectories in the absence of disturbances yields

$$\dot{V}_z = \sigma_z \dot{\sigma}_z = -\beta_z \sigma_z \text{sgn}(\sigma_z) = -\beta_z |\sigma_z|. \tag{31}$$

If the switching magnitude is selected as $\beta_z \geq {}^{\alpha}/_{\sqrt{2}}$, where α is a positive constant, the upper bound on $\dot{V}_z$ is

$$\dot{V}_z \leq -\frac{\alpha}{\sqrt{2}}|\sigma_z| = -\alpha V_z^{\frac{1}{2}}, \tag{32}$$

ensuring the convergence of the system trajectories to the sliding manifold (28) in finite-time

$$t_f = \frac{\sqrt{2}}{\alpha}\sigma_z(0). \tag{33}$$

Hence, the SOSM based altitude controller of the quadrotor UAV is designed using (30), where $\dot{\sigma}_z$ is expressed by derivative of (27) as

$$\dot{\sigma}_z = \ddot{e}_z + \frac{c_z\dot{e}_z}{2|e_z|^{\frac{1}{2}}} = \dddot{z} - \dddot{z}_{ref} + \frac{c_z\dot{e}_z}{2|e_z|^{\frac{1}{2}}}. \tag{34}$$

Second derivative of the quadrotor altitude is obtained by deriving (16) as

$$\begin{aligned}\ddot{z} = &-c_\theta\dot{\theta}u - s_\theta\dot{u} - s_\phi s_\theta\dot{\theta}v + c_\phi c_\theta\dot{\phi}v + s_\phi c_\theta\dot{v} + \\ &- c_\phi s_\theta\dot{\theta}w - s_\phi c_\theta\dot{\phi}w + c_\phi c_\theta\dot{w}.\end{aligned} \tag{35}$$

Substituting $\dot{w}$ from (19) in (35) yields

$$\begin{aligned}\dot{\sigma}_z = &-c_\theta\dot{\theta}u - s_\theta\dot{u} + \dot{A}_1 v + A_1\dot{v} + \dot{A}_2 w + \\ &+ A_2\left(Qu - Pv - gA_2 + \frac{T}{m}\right) - \dddot{z}_{ref} + \frac{c_z\dot{e}_z}{2|e_z|^{\frac{1}{2}}},\end{aligned} \tag{36}$$

where notations $A_1 = c_\theta s_\phi$ i $A_2 = c_\theta c_\phi$ are used to simplify the equations. Now, by combining (36) and (30), the thrust control law is derived as follows .

$$\begin{aligned}T = \frac{m}{A_2}\Bigg[&\dddot{z}_{ref} - \frac{c_z\dot{e}_z}{2|e_z|^{\frac{1}{2}}} + c_\theta\dot{\theta}u + s_\theta\dot{u} - \dot{A}_1 v - A_1\dot{v} \\ &- \dot{A}_2 w - A_2 Qu + A_2 Pv + A_2^2 g - \beta_z\text{sgn}(\sigma_z)\Bigg].\end{aligned} \tag{37}$$

The system trajectory can be outside the sliding surface either at the start of the transition due to initial conditions or later due to the effect of disturbances. The main task of the thrust switching control term $-\beta_z\text{sgn}(\sigma_z)$ in (37) is to ensure the convergence of the system trajectory to the sliding surface (28) and compensate for disturbances and uncertainties. Indeed, if a matched disturbance d_T affects the system through channel (19), the additional term $A_2 d_T$ will appear on the right-hand side of (36), so the upper bound on $\dot{V}_z$ can be derived as follows

$$\begin{aligned}\dot{V}_z &= \sigma_z\left[A_2 d_T - \beta_z\text{sgn}(\sigma_z)\right] \\ &\leq |A_2||d_T||\sigma_z| - \beta_z|\sigma_z| \leq |d_T||\sigma_z| - \beta_z|\sigma_z| \\ &= -\left(\beta_z - L_z\right)|\sigma_z|,\end{aligned} \tag{38}$$

where $L_z \in \mathbb{R}^+$ represents the upper bound of a disturbance d_T, i.e. $|d_T| \leq L_z$. Hence, $\dot{V}_z$ will be negative definite if the thrust switching magnitude is chosen large enough to attenuate disturbances such that $\beta_z \geq L_T + {}^{\alpha}/_{\sqrt{2}}$ holds, thus providing the finite-time convergence of the system trajectories to the sliding manifold (28).

B. SOSM based attitude control of the quadrotor UAV

This section describes the SOSM based design of the attitude control vector. It implies the design of three controllers that provide three moments τ_x, τ_y, and τ_z to reach the UAV reference orientation. Firstly, define the roll tracking error e_ϕ as the difference between the actual roll angle ϕ and the reference roll angle ϕ_{ref} as

$$e_\phi = \phi - \phi_{ref}, \tag{39}$$

and the roll sliding surface as

$$\sigma_\phi = \dot{e}_\phi + c_\phi|e_\phi|^{\frac{1}{2}}\text{sgn}(e_\phi) = 0, \tag{40}$$

where c_ϕ is a positive constant. The derivative of the sliding variable σ_ϕ from (40) yields the following

$$\dot{\sigma}_\phi = \ddot{e}_\phi + \frac{c_\phi\dot{e}_\phi}{2|e_\phi|^{\frac{1}{2}}} = \dddot{\phi} - \dddot{\phi}_{ref} + \frac{c_\phi\dot{e}_\phi}{2|e_\phi|^{\frac{1}{2}}}. \tag{41}$$

Second derivative of ϕ is obtained using (23) as follows

$$\dddot{\phi} = \dot{P} + \dot{Q}A_3 + Q\dot{A}_3 + \dot{R}A_4 + R\dot{A}_4, \tag{42}$$

where $A_3 = s_\phi t_\theta$ and $A_4 = c_\phi t_\theta$. Substituting (20) in (42) and using the condition

$$\dot{\sigma}_\phi + \beta_\phi\text{sgn}(\sigma_\phi) = 0 \tag{43}$$

for the finite-time convergence to the roll sliding surface (40), the control law for the moment around the x axis is .

$$\begin{aligned}\tau_x = &I_{XX}\Bigg[-a_1 QR + A_2 W_G Q - \dot{Q}A_3 - Q\dot{A}_3 - \\ &- \dot{R}A_4 - R\dot{A}_4 + \dddot{\phi}_{ref} - \frac{c_\phi\dot{e}_\phi}{2|e_\phi|^{\frac{1}{2}}} - \beta_\phi\text{sgn}(\sigma_\phi)\Bigg],\end{aligned} \tag{44}$$

where $a_1 = \frac{I_{YY} - I_{ZZ}}{I_{XX}}$ and $a_2 = \frac{I_{ZZM}}{I_{XX}}$ are introduced to shorten the notation. To compensate for the matched disturbance d_{τ_x} and other uncertainties that affect the system through the channel (20), the switching control parameter $\beta_\phi \in \mathbb{R}^+$ should be selected such that $\beta_\phi \geq L_\phi + {}^{\alpha}/_{\sqrt{2}}$ holds, where $L_\phi \in \mathbb{R}^+$ is the upper bound of disturbance d_{τ_x}, that is, $|d_{\tau_x}| \leq L_\phi$.

The SOSM based controllers for τ_y and τ_z can be synthesized in a similar way to previously described procedures for the design of thrust T and moment τ_x as follows: .

$$\begin{aligned}\tau_y = &\frac{I_{YY}}{c_\phi}\Bigg[\ddot{\theta}_{ref} - \frac{c_\theta\dot{e}_\theta}{2|e_\theta|^{\frac{1}{2}}} - b_1 PRc_\phi - b_2 PW_G c_\phi + \\ &+ Qs_\phi\dot{\phi} + \dot{R}s_\phi + Rc_\phi\dot{\phi} - \beta_\theta\text{sgn}(\sigma_\theta)\Bigg], \\ \tau_z = &\frac{I_{ZZ}}{A_6}\Bigg[\dddot{\psi}_{ref} - \frac{c_\psi\dot{e}_\psi}{2|e_\psi|^{\frac{1}{2}}} - Q\dot{A}_5 - \dot{Q}A_5 - R\dot{A}_6 - \\ &- d_1 PQA_6 - \beta_\psi\text{sgn}(\sigma_\psi)\Bigg],\end{aligned} \tag{45}$$

where $b_1 = \frac{I_{ZZ} - I_{XX}}{I_{YY}}$, $b_2 = \frac{I_{ZZM}}{I_{YY}}$, $A_5 = \frac{s_\phi}{c_\theta}$, $A_6 = \frac{c_\phi}{c_\theta}$, and $d_1 = \frac{I_{XX} - I_{YY}}{I_{ZZ}}$ are used to shorten the equations. Control parameters c_θ and c_ψ represent positive constants, while pitch and yaw switching magnitudes should be selected large enough to compensate for matched disturbances d_{τ_y} and d_{τ_z}, with upper bounds L_θ and L_ψ, respectively, such that $\beta_\theta \geq L_\theta + {}^{\alpha}/_{\sqrt{2}}$ and $\beta_\psi \geq L_\psi + {}^{\alpha}/_{\sqrt{2}}$ hold.

IV. SIMULATION RESULTS

This section presents, through different demonstration scenarios, the robustness properties of the SOSMC designed in the previous section to track the reference trajectories of the quadrotor UAV. The simulations are performed in *Simulink* using a fixed time step $T_s = 1\,[\text{ms}]$. The results were compared with those obtained using the FOSMC designed in [31] and showed the most promising tracking performance and robustness properties. Performance comparison analysis using SOSMC and FOSMC will be illustrated on a generalized UAV model using the same quadrotor and FOSMC parameters as in [31]. The following SOSMC parameters are used: $c_z = 17, c_\phi = 5, c_\theta = 5, c_\phi = 10$, $\beta_z = 100$, $\beta_\phi = 8$, $\beta_\theta = 8$, $\beta_\psi = 0.3$. These parameters were selected experimentally, using the *trial and error* method.

A. Comparison analysis of the quadrotor trajectory tracking in the absence of external disturbances

The first simulation scenario demonstrates the performance of SOSMC and FOSMC in tracking the UAV's trajectory when faced with the perturbation of initial conditions, but without any external disturbances. However, the SOSMC exhibits a significant improvement in the convergence of the quadrotor altitude to its reference value. Fig. 3 illustrates that both control strategies, FOSMC and SOSMC, ensure finite-time convergence of the system trajectories to the sliding manifolds. Fig. 4 depicts that SOSMC improves quadrotor performance, as it takes less time to reach the desired value of z (height), which is the coordinate at which the initial position perturbation was performed. Unlike FOSMC, all reference values are reached in finite time using SOSMC. Fig. 5 shows an asymptotic convergence of the first derivative of altitude and orientation tracking errors provided by both controllers. Additionally, it can be observed that all first derivatives of the tracking errors converge to zero within a short period, and after 3 seconds, all signals are in the vicinity of equilibrium. Only in the case of FOSMC, it takes longer (around 8.5 seconds) for the first derivative of the altitude tracking error to reach equilibrium. Fig. 6 shows control signals, and it is noticeable that both controllers need a lot of power and have roughly the same control action.

B. Comparison analysis of the quadrotor trajectory tracking in the presence of external disturbances

The second simulation scenario introduces a matched vanishing disturbance $d_3(t) = s(t) - s(t-1)$ through the state channel (19), where $s(t)$ denotes the step signal. A more challenging reference trajectory is used, called *Vivian*, but without perturbing the initial conditions of the quadrotor. Fig. 7 shows that both controllers are able to easily maintain the robust stability of the closed-loop system in the presence of vanishing disturbance, but without perturbation of initial conditions.

A non-vanishing disturbance $d_4(t) = 2.5\sin(3t)$ is introduced in the third simulation scenario. The disturbance is added to the system through channels (20), (21), (22), (23) and (24), thus representing a combined influence of matched and mismatched disturbances. Fig. 8 shows the improved tracking performance of SOSMC, since FOSMC exhibits slight oscillations around the reference trajectory, which is a consequence of a lower attenuation of the mismatched disturbance. However, it can be observed in Fig. 9 that the quadrotor tracking errors converge to zero very quickly, although certain oscillations of small amplitude are still noticeable in the quadrotor altitude when using FOSMC.

C. Comparison analysis of the quadrotor trajectory tracking using HGA

As evidenced in previous simulation scenarios, SOSMC has demonstrated improved robustness properties and superior tracking performance compared to FOSMC. However, it should be noted that both controllers manifest a chattering effect within their control signals. Reducing the chattering phenomenon can be performed by finding the mean value of the switching control term in the SMs. Therefore, SOSMC-HGA will act the same as the convenient SOSMC when trajectories are not on the sliding surface and is hence implemented as

$$u = \begin{cases} \hat{u}_{eq} + u_{conv}, & \text{for } |\sigma| > \sigma_d, \\ \hat{u}_{eq} + LPF(u_{conv}), & \text{for } |\sigma| \leq \sigma_d, \end{cases} \tag{46}$$

where $\sigma_d = 0.1$ is a constant experimentally determined to be located in the vicinity of the sliding manifold, and $G_{LPF}(s) = \frac{K}{Ts+1}$ is a transfer function of the low-pass filter (LPF). LPF parameters are selected separately for each of the four controlled variables as follows: $K_z = 0.2$, $K_\phi = 0.01$, $K_\theta = 0.01$, $K_\psi = 0.088$, $T_z = 0.04$, $T_\phi = 0.0004$, $T_\theta = 0.0004$, $T_\psi = 0.00007$. In Fig. 10 it is shown that SOSMC-HGA robustly stabilizes the closed-loop system, providing similar results to SOSMC in simulation scenario 3. In Fig. 11 it is shown that the sliding variables are smoother and converge to zero in finite time. Nevertheless, the main contribution of SOSMC-HGA is illustrated in Fig. 12. Control signals now contain significantly less chattering, which is a key advancement, since it increases the safety and reduces the power consumed by UAVs.

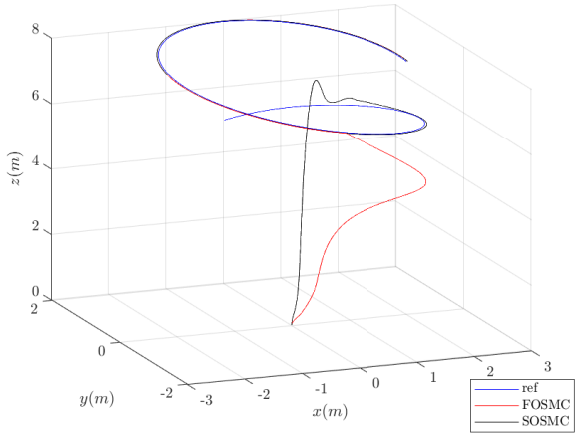

Fig. 2: Trajectory tracking of the quadrotor (simulation scenario 1)

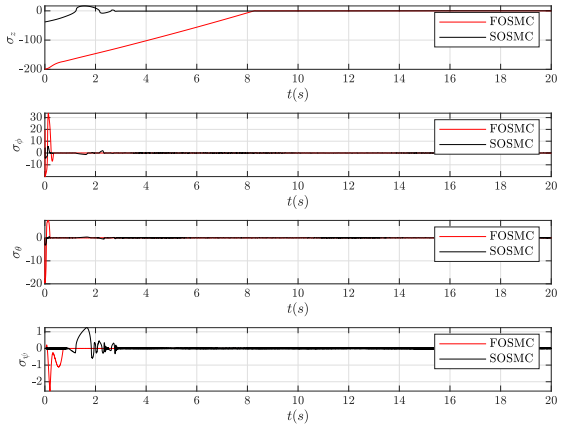

Fig. 3: Sliding variables (simulation scenario 1)

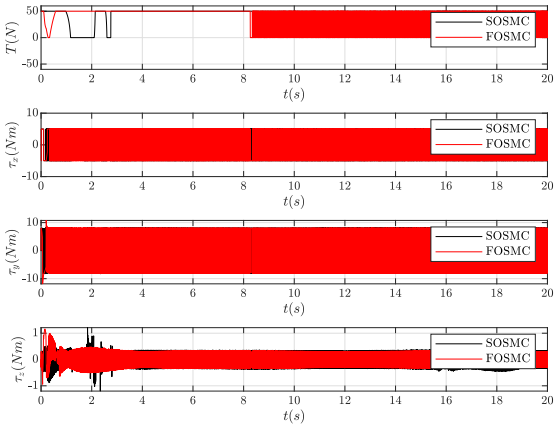

Fig. 6: Control signals (simulation scenario 1)

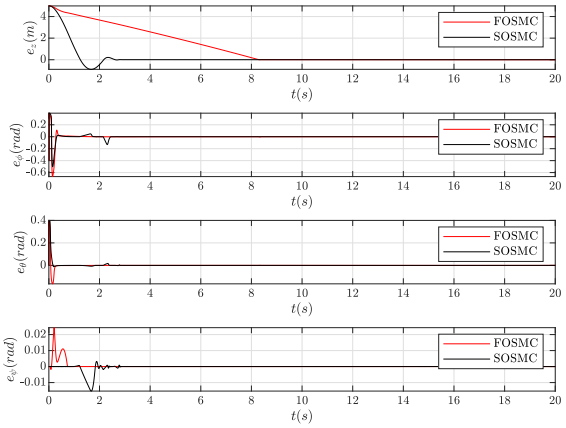

Fig. 4: Tracking errors of the quadrotor outputs (simulation scenario 1)

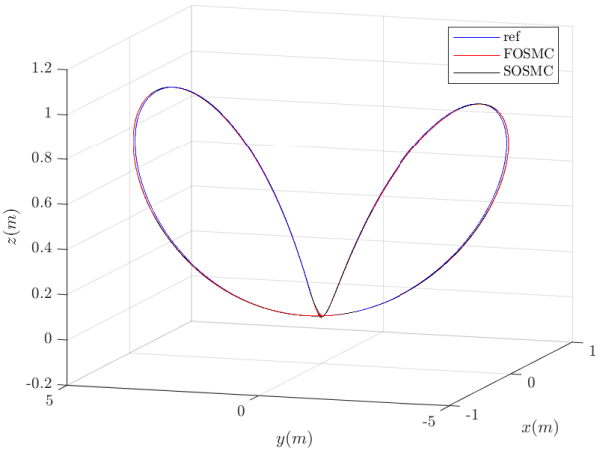

Fig. 7: Trajectory tracking of the quadrotor (simulation scenario 2)

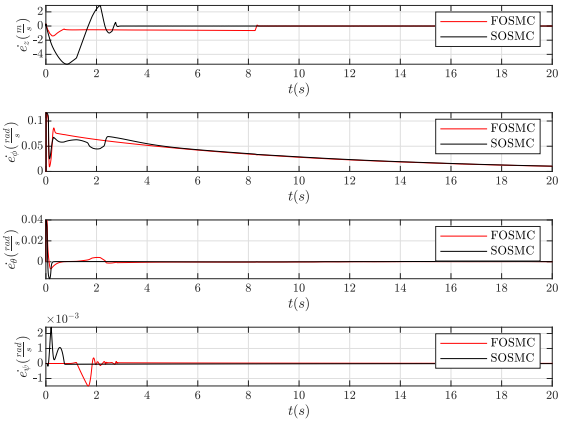

Fig. 5: First order derivatives of output tracking errors (simulation scenario 1)

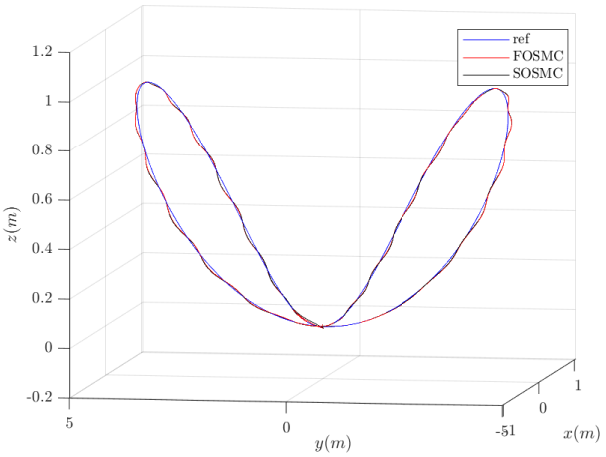

Fig. 8: Trajectory tracking of the quadrotor (simulation scenario 3)

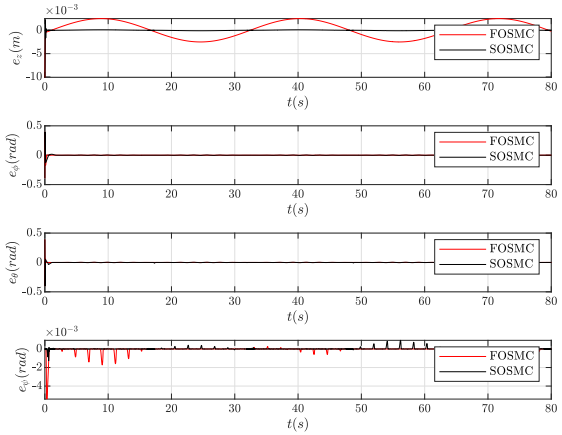

Fig. 9: Tracking errors of the quadrotor outputs (simulation scenario 3)

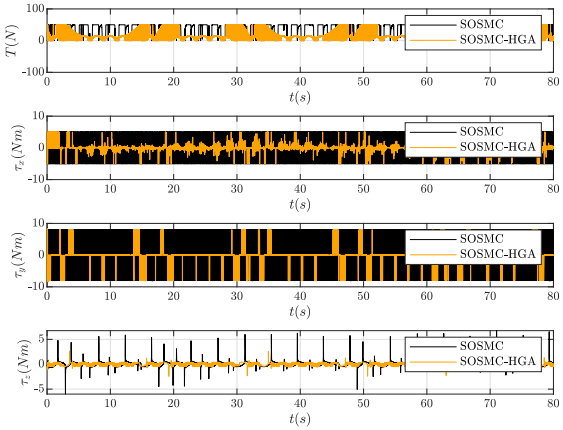

Fig. 12: Control signals (simulation scenario 3)

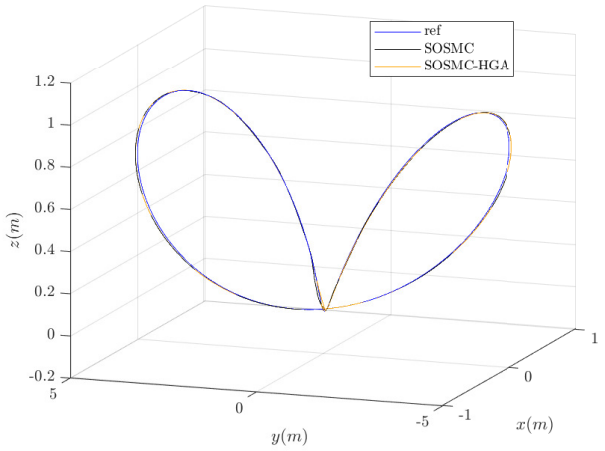

Fig. 10: The quadrotor trajectory tracking (simulation scenario 3)

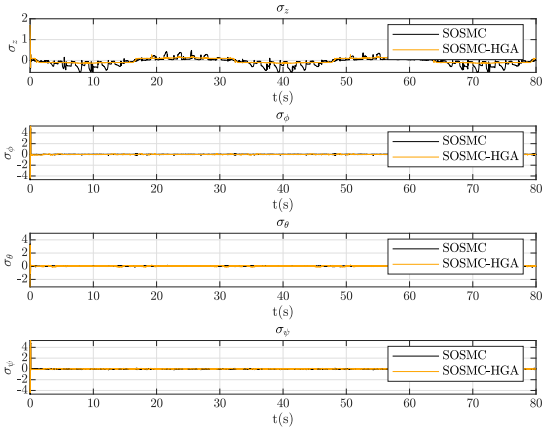

Fig. 11: Sliding variables (simulation scenario 3)

V. CONCLUSIONS

This paper presents the SOSMC design to robustly stabilize the highly nonlinear and underactuated quadrotor UAV in the presence of modeling uncertainties and bounded external disturbances. The SOSMC is able to drive the quadrotor UAV to a desired 3D trajectory, maintaining the reference position and orientation. The stability analysis performed shows that the proposed SOSMC ensures finite-time convergence of the quadrotor UAV trajectories to the sliding surfaces and finite-time convergence of its tracking errors to the origin. The SOSMC design for the quadrotor UAV is simplified using the flat mapping between the Euler and Cartesian coordinates. A notable attenuation of the chattering phenomenon is achieved by adopting the HGA algorithm in the SOSMC scheme. Simulation studies have shown that the designed SOSMC and SOSMC-HGA exhibit enhanced robustness properties and tracking performance of the quadrotor UAV compared to competitive methods. This improvement is especially evident in the significant decrease in the convergence time of the UAV altitude, which is one of the most important parameters.

REFERENCES

[1] S. Bouabdallah, A. Noth, and R. Siegwart, "Pid vs lq control techniques applied to an indoor micro quadrotor," in *2004 IEEE/RSJ International Conference on Intelligent Robots and Systems (IROS)(IEEE Cat. No. 04CH37566)*, vol. 3. IEEE, 2004, pp. 2451–2456.

[2] R. Mahony, V. Kumar, and P. Corke, "Multirotor aerial vehicles: Modeling, estimation, and control of quadrotor," *IEEE Robotics & Automation Magazine*, vol. 19, no. 3, pp. 20–32, 2012.

[3] A. Salihbegovic, E. Sokic, N. Osmic, and M. Hebibovic, "High performance disturbance observer based control of the nonlinear 2dof helicopter system," in *2013 XXIV International Conference on Information, Communication and Automation Technologies (ICAT)*, 2013, pp. 1–7.

[4] A. Salihbegovic and M. Hebibovic, "Attitude tracking of the small-scale helicopter system using disturbance observer based sliding mode control," in *22nd Mediterranean Conference on Control and Automation*, 2014, pp. 1578–1583.

[5] A. Salihbegovic, M. Hebibovic, and E. Sokic, "Synthesis of the integral sliding mode control and the robust internal-loop compensator for a class of nonlinear systems with matched uncertainties," in *2015 XXV International Conference on Information, Communication and Automation Technologies (ICAT)*, 2015, pp. 1–8.

[6] R. Xu and U. Ozguner, "Sliding mode control of a quadrotor helicopter," in *Proceedings of the 45th IEEE Conference on Decision and Control*, 2006, pp. 4957–4962.

[7] S. Bouabdallah and R. Siegwart, "Backstepping and sliding-mode techniques applied to an indoor micro quadrotor," in *Proceedings of the 2005 IEEE international conference on robotics and automation*. IEEE, 2005, pp. 2247–2252.

[8] S. Lupashin, M. Hehn, M. W. Mueller, A. P. Schoellig, M. Sherback, and R. D'Andrea, "A platform for aerial robotics research and demonstration: The flying machine arena," *Mechatronics*, vol. 24, no. 1, pp. 41–54, 2014.

[9] D. Mellinger, N. Michael, and V. Kumar, "Trajectory generation and control for precise aggressive maneuvers with quadrotors," *The International Journal of Robotics Research*, vol. 31, no. 5, pp. 664–674, 2012.

[10] G. Lu, W. Xu, and F. Zhang, "On-manifold model predictive control for trajectory tracking on robotic systems," *IEEE Transactions on Industrial Electronics*, vol. 70, no. 9, pp. 9192–9202, 2023.

[11] R. Ritz, M. W. Müller, M. Hehn, and R. D'Andrea, "Cooperative quadrocopter ball throwing and catching," in *2012 IEEE/RSJ International Conference on Intelligent Robots and Systems*. IEEE, 2012, pp. 4972–4978.

[12] D. Lee, T. Ryan, and H. J. Kim, "Autonomous landing of a vtol uav on a moving platform using image-based visual servoing," in *2012 IEEE International Conference on Robotics and Automation*, 2012, pp. 971–976.

[13] S. Shen, N. Michael, and V. Kumar, "Autonomous multi-floor indoor navigation with a computationally constrained mav," in *2011 IEEE International Conference on Robotics and Automation*. IEEE, 2011, pp. 20–25.

[14] S. Shen, Y. Mulgaonkar, N. Michael, and V. Kumar, "Multi-sensor fusion for robust autonomous flight in indoor and outdoor environments with a rotorcraft mav," in *2014 IEEE International Conference on Robotics and Automation (ICRA)*. IEEE, 2014, pp. 4974–4981.

[15] N. Michael, D. Mellinger, Q. Lindsey, and V. Kumar, "The grasp multiple micro-uav testbed," *IEEE Robotics & Automation Magazine*, vol. 17, no. 3, pp. 56–65, 2010.

[16] T. Tomic, K. Schmid, P. Lutz, A. Domel, M. Kassecker, E. Mair, I. L. Grixa, F. Ruess, M. Suppa, and D. Burschka, "Toward a fully autonomous uav: Research platform for indoor and outdoor urban search and rescue," *IEEE robotics & automation magazine*, vol. 19, no. 3, pp. 46–56, 2012.

[17] I. Golightly and D. Jones, "Visual control of an unmanned aerial vehicle for power line inspection," in *ICAR'05. Proceedings., 12th International Conference on Advanced Robotics, 2005.* IEEE, 2005, pp. 288–295.

[18] Z. Li, Y. Liu, R. Hayward, J. Zhang, and J. Cai, "Knowledge-based power line detection for uav surveillance and inspection systems," in *2008 23rd International Conference Image and Vision Computing New Zealand*. IEEE, 2008, pp. 1–6.

[19] J. Martinez-De Dios and A. Ollero, "Automatic detection of windows thermal heat losses in buildings using uavs," in *2006 world automation congress*. IEEE, 2006, pp. 1–6.

[20] C. Zhang and J. M. Kovacs, "The application of small unmanned aerial systems for precision agriculture: a review," *Precision agriculture*, vol. 13, pp. 693–712, 2012.

[21] F. Fraundorfer, L. Heng, D. Honegger, G. H. Lee, L. Meier, P. Tanskanen, and M. Pollefeys, "Vision-based autonomous mapping and exploration using a quadrotor mav," in *2012 IEEE/RSJ International Conference on Intelligent Robots and Systems*. IEEE, 2012, pp. 4557–4564.

[22] M. Blösch, S. Weiss, D. Scaramuzza, and R. Siegwart, "Vision based mav navigation in unknown and unstructured environments," in *2010 IEEE International Conference on Robotics and Automation*, 2010, pp. 21–28.

[23] T. Krajník, V. Vonásek, D. Fišer, and J. Faigl, "Ar-drone as a platform for robotic research and education," in *Research and Education in Robotics-EUROBOT 2011: International Conference, Prague, Czech Republic, June 15-17, 2011. Proceedings*. Springer, 2011, pp. 172–186.

[24] R. Xu and Ümit Özgüner, "Sliding mode control of a class of underactuated systems," *Automatica*, vol. 44, no. 1, pp. 233–241, 2008.

[25] H. Wang, X. Ye, Y. Tian, G. Zheng, and N. Christov, "Model-free–based terminal smc of quadrotor attitude and position," *IEEE Transactions on Aerospace and Electronic Systems*, vol. 52, no. 5, pp. 2519–2528, 2016.

[26] F. Chen, R. Jiang, K. Zhang, B. Jiang, and G. Tao, "Robust backstepping sliding-mode control and observer-based fault estimation for a quadrotor uav," *IEEE Transactions on Industrial Electronics*, vol. 63, no. 8, pp. 5044–5056, 2016.

[27] H. Ríos, R. Falcón, O. A. González, and A. Dzul, "Continuous sliding-mode control strategies for quadrotor robust tracking: Real-time application," *IEEE Transactions on Industrial Electronics*, vol. 66, no. 2, pp. 1264–1272, 2019.

[28] B. Mu, K. Zhang, and Y. Shi, "Integral sliding mode flight controller design for a quadrotor and the application in a heterogeneous multi-agent system," *IEEE Transactions on Industrial Electronics*, vol. 64, no. 12, pp. 9389–9398, 2017.

[29] N. Osmic, A. Tahirovic, and I. Petrovic, "Risk-sensitive motion planning for mavs based on mission-related fault-tolerant analysis," *Automatika*, vol. 61, no. 2, pp. 295–311, 2020.

[30] N. Osmic, A. Tahirovic, and B. Lacevic, "Octocopter design: Modelling, control and motion planning," *arXiv preprint arXiv:2212.01210*, 2022.

[31] A. Salihbegovic, A. Talic, N. Osmic, and E. Sokic, "3d trajectory tracking of a quad-rotor unmanned aerial vehicle via the first order sliding mode control," in *2023 9th International Conference on Control, Decision and Information Technologies (CoDIT)*, 2023, pp. 1530–1535.

[32] A. Salihbegovic, V. Capin, E. Sokic, and N. Osmic, "Trajectory tracking of the octo-rotor unmanned aerial vehicle exposed to parametric uncertainties and external disturbances using first order sliding mode control," in *2023 XXIX International Conference on Information, Communication and Automation Technologies (ICAT)*, 2023, pp. 1–8.

[33] B. Tian, L. Liu, H. Lu, Z. Zuo, Q. Zong, and Y. Zhang, "Multivariable finite time attitude control for quadrotor uav: Theory and experimentation," *IEEE Transactions on Industrial Electronics*, vol. 65, no. 3, pp. 2567–2577, 2018.

[34] B. Tian, J. Cui, H. Lu, Z. Zuo, and Q. Zong, "Adaptive finite-time attitude tracking of quadrotors with experiments and comparisons," *IEEE Transactions on Industrial Electronics*, vol. 66, no. 12, pp. 9428–9438, 2019.

[35] Q. Lu, B. Ren, and S. Parameswaran, "Uncertainty and disturbance estimator-based global trajectory tracking control for a quadrotor," *IEEE/ASME Transactions on Mechatronics*, vol. 25, no. 3, pp. 1519–1530, 2020.

[36] A. Salihbegovic, "Robust internal-loop compensator based sliding mode control of nonlinear systems in the presence of mismatched disturbances," *IEEE Access*, vol. 7, pp. 50 492–50 502, 2019.

[37] J. Velagić, N. Osmić, V. Klovo, and H. Lačević, "Design of lqr controller for 3d trajectory tracking of octocopter unmanned aerial vehicle," in *2022 8th International Conference on Control, Decision and Information Technologies (CoDIT)*, vol. 1, 2022, pp. 63–68.